PIV measurement of distributed combustion without air dilution

D. Csemány[1], Á. B. Hirják[1], A. Nagy[2], A. Guba[2], V. Józsa[1,*]

[1] Department of Energy Engineering, Faculty of Mechanical Engineering, Budapest University of Technology and Economics, 1111 Budapest, Műegyetem rkp. 3., Hungary

[2] Eötvös Loránd Research Network, Centre for Energy Research, 1121 Budapest Konkoly-Thege Miklós út 29-33., Hungary

Abstract

Chemical energy carriers will play a significant role in the global energy portfolio even after reaching climate neutrality. Therefore, advanced, fuel-flexible, ultra-low emission, robust combustion concepts are highly desired for both current and future applications. Our research group introduced the Mixture Temperature-Controlled combustion concept in recent years, which requires no air dilution while offering similar characteristics to Moderate or Intense, Low-oxygen Dilution combustion. The present paper uses Particle Image Velocimetry to focus on the flow field analysis. It was concluded that the flow field is the superposition of the characteristics of a cold free jet and a homogeneous reaction zone distributed across the combustion chamber.

Introduction

Currently, 84% of our energy use is related to combustion, which includes 0.65% biofuels, i.e., mostly biodiesel and ethanol for reciprocating engines, and 6.30% traditional biomass [1]. Therefore, reaching climate neutrality requires significant effort in the upcoming decades. Global carbon neutrality will possibly not be reached by the end of this century [2,3]. There are fields where carbon-free operation can be easily reached, such as buildings. Proper insulation, photovoltaic cells, heat pumps, and split air conditioning may deliver all the required heating and cooling for most homes in the temperate climate zone. With technological advancements, the overall carbon footprint of a building can be further reduced. In contrast, there is no carbon-neutral answer for the 100 EJ problem presently, which was the total energy consumption of the transportation sector in 2014 [4]. Therefore, chemical energy carriers will dominate intercontinental transport and aviation [5]. The rest of the energy-intensive sectors scatter between these two extreme examples. Consequently, combustion research should continue the advancements aimed for in the past for clean operation [6], while being open for scaling up the operation on uncommon fuels in the industry, such as hydrogen [7] and ammonia [8].

Currently, the most researched ultra-low emission combustion technique is Moderate or Intense, Low-oxygen Dilution (MILD) combustion. It can be economically achieved by flue gas recirculation on a practical scale. However, MILD combustion is not an option in, e.g., gas turbines [9]. It is important to note that MILD combustion mimics the theoretically best scenario: combustion of a homogeneous mixture with even heat release. This is why flue gas recirculation is needed; reactions at reduced speed allow heterogeneous mixture formation before ignition.

Slowing the reactions can also be achieved by cooling down the mixture since ignition delay time is exponentially related to the local temperature [10]. This phenomenon is exploited by the recently introduced Mixture Temperature-Controlled (MTC) combustion concept [11], offering similarly low emissions, freedom from thermoacoustic oscillations [12], and a similar flame structure to MILD combustion but without the need for oxidizer dilution. Therefore, this concept has significant potential in the industry, especially for gas turbines, due to the robust and versatile nature of MTC combustion.

To better understand distributed flames, Particle Image Velocimetry (PIV) is often used to analyze the flow field and turbulent properties [13]. Even though the entire flow field cannot be captured due to physical obstacles in the path of the laser sheet, the high-gradient regions provide essential information for numerical model validation [14], which is the vicinity of the burner. Liquid fuel combustion is more complex than gaseous fuel combustion. Therefore, complete identification of the interacting processes requires the simultaneous use of advanced optical techniques, such as OH-Planar Laser-Induced Fluorescence and Phase Doppler Anemometry, besides PIV, to address them properly [15]. Even though liquid fuel was tested in the present study, atomization, droplet evaporation, and mixing occurred upstream of the flame front, allowing the decoupling mixture preparation from the ignition, making the case similar to gaseous fuel combustion. Hence, proper velocity field characterization can be performed only by PIV.

The novelty of the present research is the analysis of distributed combustion by the PIV technique of an MTC burner at selected operating conditions. Our hypothesis is the following. Once distributed combustion is achieved, the inlet boundary conditions have a minor influence on the global flow field since the delayed mixture ignition decouples the effect of atomization and evaporation on the operation, a unique feature among liquid-fueled burners.

* Corresponding author: jozsa@energia.bme.hu

Materials and methods

The measurement setup is shown in Fig. 1. Since the measurements of [11] were repeated here, the pollutant emission analysis and several features of the test rig are omitted now.

The burner features a plain-jet airblast atomizer with a 1.2 mm inner diameter of the central pipe for the liquid fuel, which was standard diesel fuel (EN590:2017) in all the test cases. The thermal power was uniformly 13.35 kW. The atomizing air discharged from a concentric annulus with 1.5 mm inner and 2.2 mm outer diameter, and the tested atomizing gauge pressures, p_g, were 0.6, 0.75, and 0.9 bar. The combustion air was preheated to two temperatures, T_{ca} = 200 °C and 250 °C, then entered the chamber via eight 45° swirl vanes in an annular channel with 21 mm inner and 40 mm outer diameter. The flue gas oxygen concentration was 7 V/V%, equal to an equivalence ratio of 0.67.

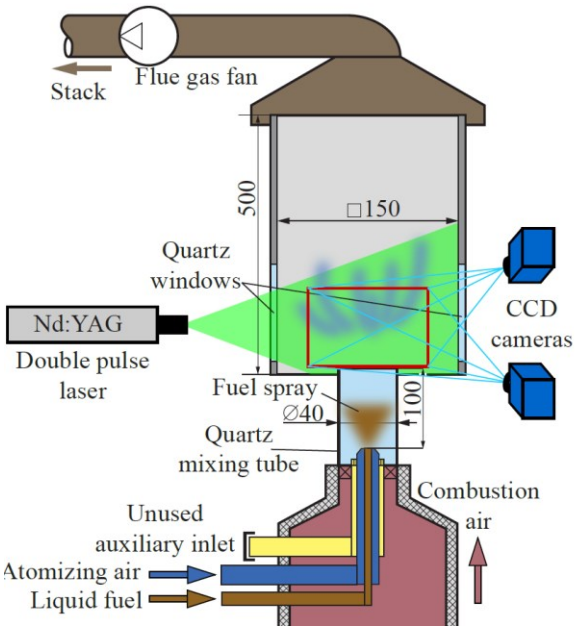

Fig. 1. Schematic of the measurement setup.

The operational parameters, along with estimated ones, are shown in Table 1, which are the geometric swirl number (S) [16] and the Sauter Mean Diameter (SMD) [12]. The Reynolds number was in the range of 10,000 inside the mixing tube, resulting in entirely turbulent flow and hence turbulent combustion.

Table 1. Key operational parameters.

Thermal power	13.35 kW
Combustion air temperature	200, 250 °C
Atomizing gauge pressure	0.6, 0.75, 0.9 bar
Sauter Mean Diameter	24.1, 21.8, 20.1 µm
Swirl number	0.08–0.13

S did not exceed 0.3 [17] or 0.6 [18], which are often treated as the critical values required for the formation of V-shaped flames. However, without liquid fuel inlet, S = 0.79 based on the swirler geometry. Therefore, V-shaped flames are possible with this burner with reduced p_g values.

The PIV measurements were performed at a 15 Hz repetition rate in a Stereo PIV configuration with a system manufactured by LaVision. A Litron PIV nano laser at 85.05 mJ/pulse/cavity set value (the peak performance is 135 mJ/pulse/cavity) was used for the measurements with two 4 MPixel LaVision Imager SX cameras. These were equipped with 532 nm ±10 nm filters to cancel the external noise. A total of 300 image pairs were recorded at each measurement point. The 15 Hz repetition rate is low for detailed flame evolution tracking while suitable for analyzing instantaneous results and statistical properties, which are presented in this paper. The flow was seeded with TiO_2 particles using a LaVision Particle Blaster 110. The seeder injection port was below the swirl vanes to have sufficient mixing with the combustion air. The combustion air flow rate was slightly decreased when injection started to maintain the constant equivalence ratio. The red frame in Fig. 1 shows the captured regime by the PIV cameras, which is just above the burner lip. Therefore, the bias due to laser light reflection and refraction was minimal.

Flame images were recorded at each setup using a Nikon D7500 commercial digital camera at f/3.5, 1/200 s exposure time, and ISO 6400 sensitivity with a fixed 35 mm f/1.8 lens. Flow seeding was turned off during image recording with the digital camera. Like the PIV cameras, the digital camera recorded the flame from the front side.

The processed PIV data from the two image pairs were exported from the DaVis 8 software, and further processing was performed in Matlab [19]. A challenge was resolving distributed combustion since unrealistic local peaks and igniting small fluid packets behave similarly. The spatial size of the latter is larger; hence, a 5×5 median filter was applied to each velocity component matrix.

Results and discussion

The flame images by the digital camera are shown in Fig. 2. Distributed combustion was entirely free from yellow flares, which indicates burning droplets and a locally inhomogeneous mixture. The images in Fig. 2 were the brightest ones from a series of recordings at 8 frames/s for a couple of seconds.

The flames are qualitatively similar and occupy a similar position inside the combustion chamber in all cases. The contour of the blue region, showing the CH* chemiluminescence, varied from image to image, confirming that the distributed flame has no characteristic shape like straight or V-shaped flames. There are various-sized burning fluid packets in the flame, indicating that the ignition of the fresh mixture is not localized. Overall, the low sensitivity of the flame shape and behavior to the operating conditions implies highly flexible operation required for practical applications. Therefore, the PIV measurement and data analysis results will be presented mainly for the

extreme cases: T_{ca} = 200 °C and p_g = 0.6 bar and T_{ca} = 250 °C and p_g = 0.9 bar.

Fig. 2. Flame images of distributed combustion. Top row: T_{ca} = 200 °C, bottom row: T_{ca} = 250 °C. Left to right: p_g = 0.6, 0.75, and 0.9 bar.

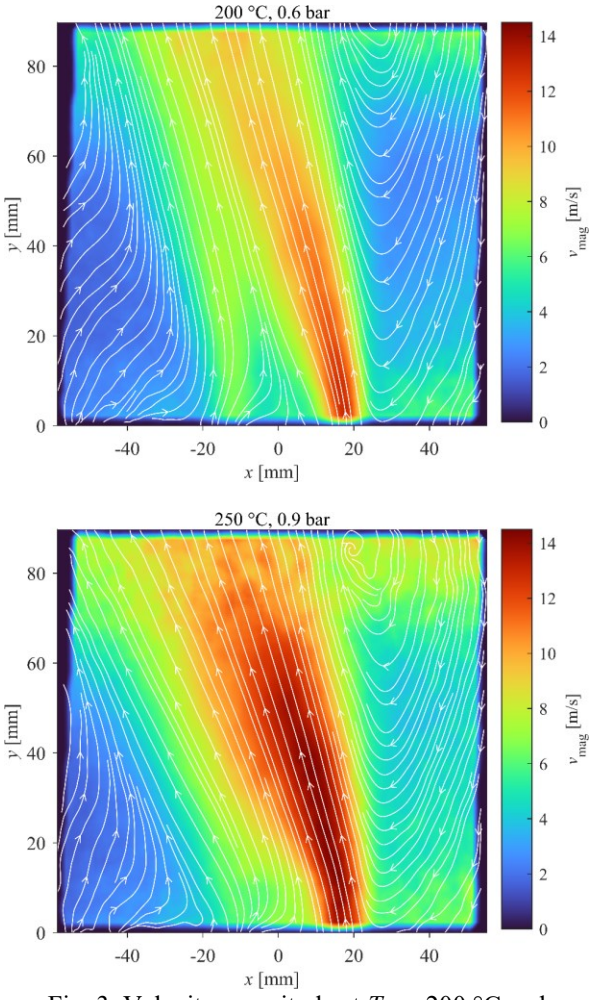

Fig. 3. Velocity magnitude at T_{ca} = 200 °C and p_g = 0.6 bar (top) and T_{ca} = 250 °C and p_g = 0.9 bar (bottom).

The mean velocity field is shown in Fig. 3. The 114×90 mm region highlights the discharging cold mixture and the lower region of the reaction zone. Recirculation is visible on both sides, with a larger zone on the right. MILD combustion requires about recirculated mass flow ratio of two [20]. However, it peaked at 0.3 for the presented burner and combustion chamber configuration [21], which is closely a magnitude difference. It means that the presented combustion is notably different from MILD combustion systems; nevertheless, both operate in distributed combustion mode.

Negative v_y was only observed on the right side of the plots of Fig. 3, starting from x = 26 mm. Mean v_y was varied between -2.1 and 12.4 m/s. Even though the zone on the left side of the mixture jet featured vortices and negative v_y values, the mean of the 300 image pairs was uniformly positive in this region.

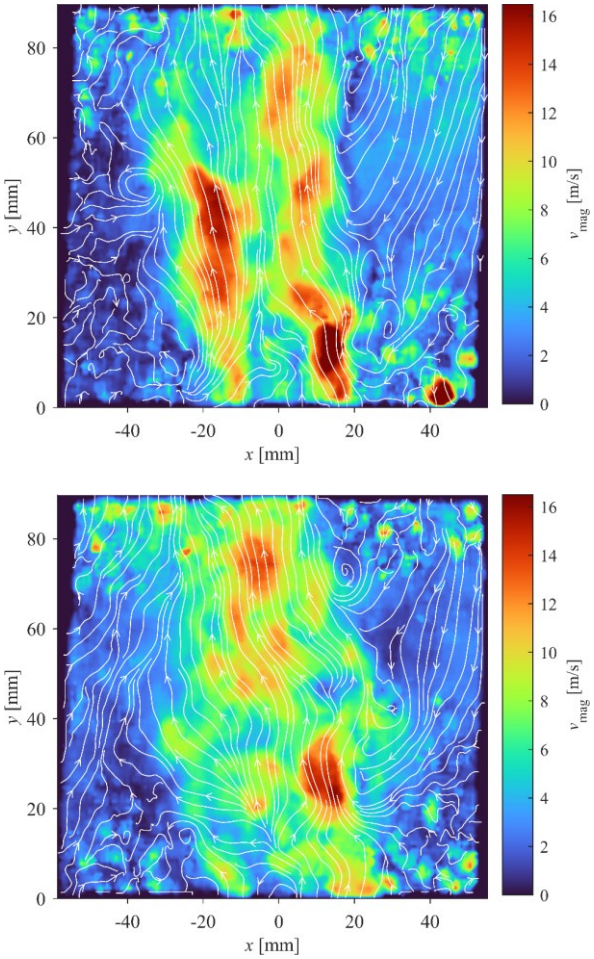

Fig. 4. Instantaneous velocity fields of two subsequent images at T_{ca} = 200 °C and p_g = 0.6 bar.

The inner and outer recirculation zones, typical in swirl combustion, are absent since the precessing vortex core was blown away. The flow field was dominated by the upstream cold mixture that ignited well downstream of the burner outlet, allowing more time for droplet evaporation, mixing with air, and igniting the more homogeneous mixture. This is the key

requirement of the low-emission operation. The discharging jet leans to the left due to the hydrodynamic instability of the burner in these conditions. The flow field was more symmetric at lower and higher thermal power values. Such a behavior is typical in in-house developed burners [22]. The region above 70 mm at 200 °C and 0.6 bar and above y = 60 mm at 250 °C and 0.9 bar are burdened with noise caused by the igniting mixture packets in the reaction zone.

Two subsequent instantaneous velocity fields with streamlines are shown in Fig. 4. The discharging mixture shows a notable variation, and the proper tracking of the corresponding features requires a higher repetition rate by two magnitudes. However, the small burning packets in the reaction zone are slower, and hence their movement is visible. The bottom part of the images is burdened with high uncertainty since the particle concentration in these regions is low. This is also indicated by the high variation in the streamlines.

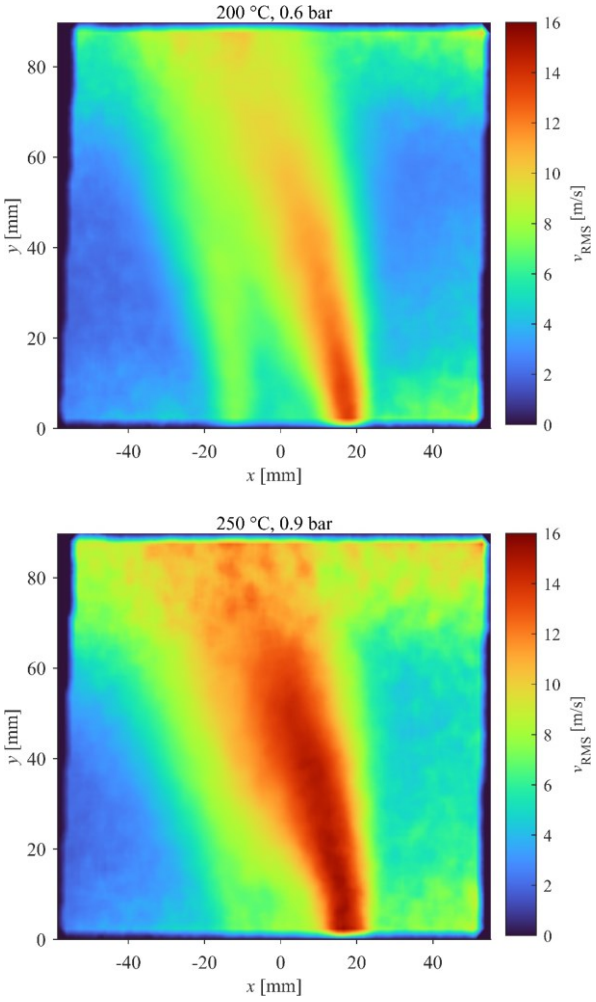

Fig. 5. RMS velocity at T_{ca} = 200 °C and p_g = 0.6 bar (top) and T_{ca} = 250 °C and p_g = 0.9 bar (bottom).

The root mean square (RMS) of the velocity field is shown in Fig. 5. The sides of the central jet showed the most intense fluctuations, similar to an isothermal free jet. Since the increased p_g leads to a more intense shear between the atomizing jet and the combustion air, the fluctuations are more intense at p_g = 0.9 bar. The relative value of the two presented cases is identical. The fluctuating part starting from 70 mm and 60 mm in the two images shows the beginning of the reaction zone. Regardless of the flow field leaning to the left, the reaction zone here is more symmetric. Since the large recirculation on the right side greatly facilitates the spreading of the cold mixture, this side shows higher fluctuations as the mixture ignites.

The bottom and side parts with higher intensity values are partially due to the recirculations shown in Fig. 3. The other reason is the low concentration of the seeding particles. The recirculation zones are more significant in the present case since the mixing tube protrusion length is 20 mm rather than flush with the combustion chamber base plate.

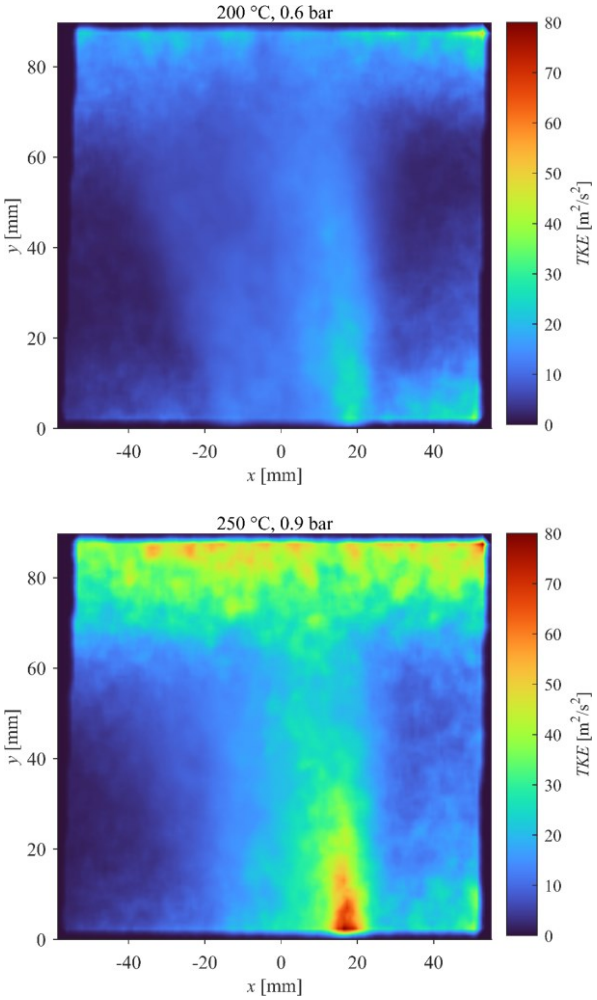

Fig. 6. Turbulence kinetic energy at T_{ca} = 200 °C and p_g = 0.6 bar (top) and T_{ca} = 250 °C and p_g = 0.9 bar (bottom).

According to our preliminary investigations on the protrusion distance, distributed combustion was only possible in a very small operating parameter range if reduced to zero. Compared to the velocity magnitude in Fig. 3, v_{RMS} is close to v_{mag} at similar positions. In the reaction zone, the fluctuating velocity is significantly larger than the mean velocity for all cases.

Figure 6 shows the turbulence kinetic energy (*TKE*). Due to the summed fluctuating velocity squares in the formula, the results are the enhanced variant of Fig. 5. The shear layer of the discharging mixture is fading to the background at p_g = 0.6 bar, while a smaller region is present at p_g = 0.9 bar right downstream the right side of the mixing tube lip. The reaction zone shows higher *TKE* in the latter case. The bottom right corner shows a high-intensity region, also in Figs. 4 and 5, where the causes were detailed.

TKE is the most suitable for reaction zone detection among all the contour plots. This is supported by the fact that the reacting turbulent flow structures will expand, accelerating the fluid packets. Since the oscillating components are considered in *TKE* on the square, it provides sufficiently high contrast. Moreover, the fluctuations and hence the *TKE* distribution of a non-reacting free jet are decreasing downstream. The amplifying fluctuations require additional energy provided by the chemical reactions in the entirely turbulent flow.

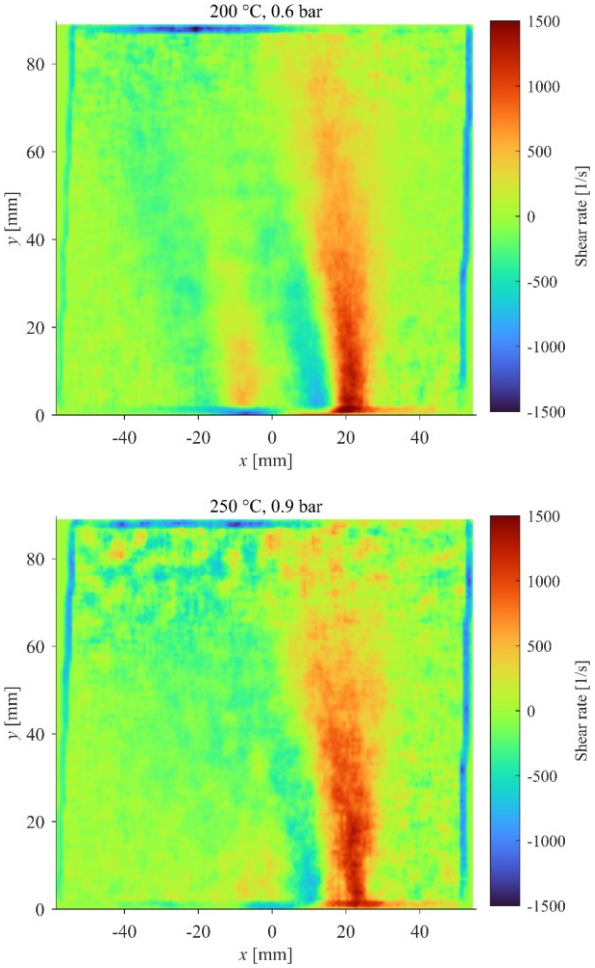

Fig. 7. Shear rate at T_{ca} = 200 °C and p_g = 0.6 bar (top) and T_{ca} = 250 °C and p_g = 0.9 bar (bottom).

The shear rate (h) is shown in Fig. 7. This is calculated as follows:

$$h = \frac{\partial v_y}{\partial x} + \frac{\partial v_x}{\partial y}. \quad (1)$$

The instantaneous values were highly scattered without informative trends. Therefore, Fig. 7 shows the mean values. The free jet boundaries are visible and more characteristic than in the case of any previous figure. The shear rate on the right side of the cold mixture jet is positive outside as the flow expands in the positive x direction. This is followed by a negative region with a smaller amplitude, and the zero region between the two clearly shows the jet boundary with no flue gas entrainment. This phenomenon is present on the other side of the jet with inverted colors and smaller amplitudes since the left boundary are less dominant. The thin zero zones of the two sides reveal the cold mixture jet core.

The shear rate does not increase spectacularly with p_g, like v_{RMS} or *TKE* in Figs. 5 and 6, respectively. However, the core is present for a longer axial distance at p_g = 0.9 bar. However, the left side of the core is not visible in this case. The shear rate in the reaction zone intensifies with p_g.

Conclusions

This paper investigated distributed combustion without air dilution by using PIV. The fuel was standard diesel fuel. The thermal power and equivalence ratio were constant while combustion air preheating temperature and atomizing air gauge pressure were varied. The following conclusions were derived.

The flame structure was similar in all cases based on digital camera pictures. The similarity was quantitatively found in the shear rate.

The reaction zone caused fluctuations in the mean velocity magnitude plots. However, fluctuations were better emphasized by the root mean square velocity distribution and spectacularly emphasized in the turbulence kinetic energy plots.

The instantaneous velocity fields showed highly fluctuating behavior in terms of velocity magnitude and coherent fluid packet sizes, while a coarse tracking of the slower igniting fluid packets was possible.

The similarities among all the cases imply flexible operation required by practical applications. For future research, operational boundaries of distributed combustion will be tested extensively.

Acknowledgments

The research reported in this paper was supported by the National Research, Development and Innovation Fund of Hungary, project №. OTKA-FK 137758, and TKP2021 Grant №. BME-NVA-02, ÚNKP-22-5-BME-304, and ÚNKP-22-3-II-BME-100 New National Excellence Program by the Ministry for Culture and Innovation of Hungary from the National Research, Development and Innovation Fund, and the János Bolyai Research Scholarship of the Hungarian Academy of Sciences.

References

[1] Ritchie H, Roser M, Rosado P. Energy Production and Consumption. Our World Data 2022. https://ourworldindata.org/energy-production-consumption (accessed January 23, 2023).

[2] Buira D, Tovilla J, Farbes J, Jones R, Haley B, Gastelum D. A whole-economy Deep Decarbonization Pathway for Mexico. Energy Strateg Rev 2021;33:100578. https://doi.org/10.1016/j.esr.2020.100578.

[3] Pan X, Wang H, Wang L, Chen W. Decarbonization of China's transportation sector: In light of national mitigation toward the Paris Agreement goals. Energy 2018;155:853–64. https://doi.org/10.1016/j.energy.2018.04.144.

[4] Hannula I, Reiner DM. Near-Term Potential of Biofuels, Electrofuels, and Battery Electric Vehicles in Decarbonizing Road Transport. Joule 2019;3:2390–402. https://doi.org/10.1016/j.joule.2019.08.013.

[5] Gota S, Huizenga C, Peet K, Medimorec N, Bakker S. Decarbonising transport to achieve Paris Agreement targets. Energy Effic 2019;12:363–86. https://doi.org/10.1007/s12053-018-9671-3.

[6] Lefebvre AH, Ballal DR. Gas turbine combustion. third. Boca Raton: CRC Press; 2010. https://doi.org/10.1201/9781420086058.

[7] Sun Y, Zhang Y, Huang M, Li Q, Wang W, Zhao D, et al. Effect of hydrogen addition on the combustion and emission characteristics of methane under gas turbine relevant operating condition. Fuel 2022;324:124707. https://doi.org/10.1016/j.fuel.2022.124707.

[8] Valera-Medina A, Xiao H, Owen-Jones M, David WIF, Bowen PJ. Ammonia for power. Prog Energy Combust Sci 2018;69:63–102. https://doi.org/10.1016/j.pecs.2018.07.001.

[9] Xing F, Kumar A, Huang Y, Chan S, Ruan C, Gu S, et al. Flameless combustion with liquid fuel: A review focusing on fundamentals and gas turbine application. Appl Energy 2017;193:28–51. https://doi.org/10.1016/j.apenergy.2017.02.010.

[10] Liu J, Hu E, Yin G, Huang Z, Zeng W. An experimental and kinetic modeling study on the low-temperature oxidation, ignition delay time, and laminar flame speed of a surrogate fuel for RP-3 kerosene. Combust Flame 2022;237:111821. https://doi.org/10.1016/j.combustflame.2021.111821.

[11] Józsa V. Mixture temperature-controlled combustion: A revolutionary concept for ultra-low NOx emission. Fuel 2021;291:120200. https://doi.org/10.1016/j.fuel.2021.120200.

[12] Józsa V, Hidegh GT, Csemány D, Kardos RA, Chong CT. Dynamics and emission of nearly flameless combustion of waste cooking oil biodiesel in an ultra-low emission non-MILD swirl burner. Fuel 2022;319:123743. https://doi.org/10.1016/j.fuel.2022.123743.

[13] Feser JS, Karyeyen S, Gupta AK. Flowfield impact on distributed combustion in a swirl assisted burner. Fuel 2020;263:116643. https://doi.org/10.1016/j.fuel.2019.116643.

[14] Brito Lopes A V., Emekwuru N, Joshi K. Are the available data from laboratory spray burners suitable for CFD modelling validations? A review. Energy Convers Manag X 2022;16:100289. https://doi.org/10.1016/j.ecmx.2022.100289.

[15] Verdier A, Marrero Santiago J, Vandel A, Godard G, Cabot G, Renou B. Local extinction mechanisms analysis of spray jet flame using high speed diagnostics. Combust Flame 2018;193:440–52. https://doi.org/10.1016/j.combustflame.2018.03.032.

[16] Beér JM, Chigier NA. Combustion aerodynamics. London: Robert E. Krieger Publishing Company, Inc.; 1972.

[17] Guiberti TF, Durox D, Zimmer L, Schuller T. Analysis of topology transitions of swirl flames interacting with the combustor side wall. Combust Flame 2014;162:4342–57. https://doi.org/10.1016/j.combustflame.2015.07.001.

[18] Lilley DG. Swirl Flows in Combustion: A Review. AIAA J 1977;15:1063–78. https://doi.org/10.2514/3.60756.

[19] MathWorks. MATLAB, Release 2022b 2022.

[20] Wünning JA, Wünning JG. Flameless oxidation to reduce thermal NO-formation. Prog Energy Combust Sci 1997;23:81–94. https://doi.org/10.1016/s0360-1285(97)00006-3.

[21] Füzesi D, Malý M, Jedelský J, Józsa V. Numerical modeling of distributed combustion without air dilution in a novel ultra-low emission turbulent swirl burner. Phys Fluids 2022;34. https://doi.org/10.1063/5.0085058.

[22] Huang M, Li R, Xu J, Cheng S, Deng H, Rong Z, et al. Effect of equivalence ratio and staging ratio on the methane MILD combustion in dual-stage combustor. Fuel 2022;307:121903. https://doi.org/10.1016/j.fuel.2021.121903.